

**CONSTRUCTION OF MARINE SURFACE PRESSURE FIELDS FROM  
SCATTEROMETER WINDS ALONE**

Carol S. Hsu\* and Morton G. Wurtele

Dept of Atmospheric Sciences

University of California, Los Angeles

Los Angeles, CA 90025

Glenn F. Cunningham and Peter M. Woiceshyn

Jet Propulsion Laboratory

California Institute of Technology

Pasadena, CA 91109

submitted to Journal of Applied Meteorology, April 1996, revised March 1997.

*Current affiliation:* Carol S. Hsu, Jet Propulsion Lab, MS 300-320

4800 Oak Grove Dr., Pasadena, CA 91109

## **abstract**

A series of six-hourly, synoptic, gridded, global surface wind fields with a resolution of 100 km has been generated using the **dataset** of **dealised** Seasat satellite scatterometer (SASS) winds produced as described by **Peteherych** et al. (1984). This paper **is** an account of the construction of surface pressure fields from these SASS synoptic wind fields only, as carried out by different methods, and the comparison of these pressure fields with U. S. National Centers for Environmental Prediction (**NCEP**) analyses, with the pressure fields of the European **Centre** for Medium Range Weather Forecasting (**ECMWF**) and with the special analyses of the Gulf of Alaska Experiment (**GOASEX**).

One of the methods we use to derive the pressure fields utilizes a two-layer planetary boundary layer (**PBL**) model iterative scheme that relates the **geostrophic** wind vector to the surface wind vector, surface roughness, humidity, **adiabatic** and **baroclinic** effects and secondary flow. A second method involves the assumption of zero **two-dimensional** divergence, leading to a Poisson equation (the 'balance equation') in pressure, with the wind field serving as a forcing function.

The pressure fields computed from the SASS winds using a two-layer PBL model closely approximate the **NMC** and ECMWF fields. In some cases, the **PBL-model-derived** pressure fields can detect **mesoscale** features not resolved in either the **NMC** or ECMWF analyses. Balanced-pressure fields are much smoother and less well resolved than the PBL-model-derived or **NMC** fields. Systematic differences between balanced pressure fields and the PBL-model-derived fields are attributed to the neglect of . horizontal divergence in the balance equation. The effect of stratification is found to produce a larger impact than secondary flow or thermal wind effects on the derived pressure fields. Inclusion of secondary flow tends to weaken both low and high pressure

centers whereas inclusion of stratification intensifies low centers and weakens high centers.

## 1. Introduction

The data gathered by the Seasat scatterometer system (SASS) represent a successful first effort to measure marine surface wind globally. Before the launch of the satellite, significant improvements in surface weather analysis and forecast skill over open ocean and coastal regions had been limited by the **sparsity** of observations. The high-resolution marine wind data produced from information gathered by the ocean-observing Seasat satellite for 96 days during 1978 greatly increased the observational coverage, most particularly the wind field over the oceans (see Fig. 1). The work done by Overland et al. (1980), and Atlas et al. (1982) clearly showed that the **scatterometer** system was highly successful in delineating surface weather patterns with significantly greater resolution than can possibly be achieved by *in situ* observational systems. A positive impact on forecast **skill** has been found in some cases when SASS winds are incorporated into numerical weather prediction models (see, for example, Duffy and Atlas 1986, Stoffelen and Cats, 1991, Lenzen et al. 1993). In the Southern Hemisphere, the differences in the forecasts with and without SASS winds can be **large** (about 20-30 mb within one day), according to Anderson et al. (1991). However, a method for the optimal assimilation of the relatively fine-scale scatterometer wind data has yet to be developed (Anderson et al. 1991). Positive impact of ERS-1 scatterometer winds has recently been demonstrated with the UKMO, GSFC, and NCEP models, and these data are currently being used operationally to improve NCEP and UKMO analyses and forecasts (Woiceshyn, 1996, personal communication ).

There are different approaches to the use of scatterometer data. One of which is that of the NCEP, which incorporate the non-synoptic swaths of wind observations into their weather prediction models according to their assimilation schemes. Another approach is to interpolate the swath wind observations in time and space, and use the resulting synoptic wind field as a valid data set in itself. This has been done, for example, in wave

hindcasting (Woiceshyn et al. 1989) and in precipitation estimate during Toga\_Coare (Hsu et al. 1997).

Surface pressure may also be computed directly from wind data by various methods. Some work has already been carried out on this problem. Pressure fields were derived by **Endlich** et al. (1981) by balancing the rotational part of the wind and the pressure field. Stratification, humidity, secondary flow and **baroclinity** are not accommodated in the balance equation, and this method requires a knowledge of the pressure at all boundary points to solve the resulting Poisson equation. Furthermore, pressure fields derived from the balance equation will not be accurate in tropical areas or within weather systems where **significant** convergence exists.

Another approach is to use a variational method to assimilate **scatterometer** winds into surface pressure fields by a reduction-rotation method. This was done by Harlan and O'Brien (1986) with the aid of two constraints: (1) minimize the difference between relative **vorticities** calculated from the data and those calculated from the variational solution, (2) minimize the average kinetic energy. This method requires a first-guess pressure field and assumes a constant turning **angle** between surface wind and **geostrophic** wind. Harlan and O'Brien recognized that more sophisticated models may be required; especially during explosive **cyclogenesis**, as in the Queen Elizabeth 11 storm case.

The pressure fields deduced by the methods mentioned above both exhibit substantial errors (up to 10 millibars) in the vicinity of a front or storm. In this paper, we use a two-layer planetary boundary layer (PBL) model (Brown and Liu 1982) to derive surface pressure fields from synoptic SASS winds. The output of this methodology is a **geostrophic** wind or pressure gradient, so that at least one reliable observation (e.g. buoy or coastal station) is required to produce the pressure field.

Cases in which an existing PBL model is used to obtain surface pressure fields from SASS winds are presented, these fields are then validated by National Centers for Environmental Prediction (NCEP) surface pressure analyses, by detailed GOASEX analyses, and by 1000 mb data from the European Center for Medium-Range Weather Forecasts. (The  $10 \times 1^\circ$  ECMWF data for 12 days in September 1978 were kindly provided by Dr. Anthony Hollingsworth, using their 1986 forecast and assimilation code.)

## 2. Data

The scatterometer radar on board the Seasat-A satellite provided global measurements of oceanic surface wind speed and direction accurate to  $\pm 2$  m/s and  $\pm 20^\circ$ , respectively (Jones et al. 1982). A 15-day subjectively dealiased asynoptic gridded dataset from asynchronous orbital data were produced with a resolution of 100 km x 100 km (Peteherych et al. 1984). Satellite cloud images are taken into account in determining the directions of wind vectors. For meteorological studies, we have converted this record into a synoptic dataset by interpolating these data in time, using a third-order polynomial scheme.

## 3. The two-layer PBL model

### *a. two-layer similarity model*

To obtain pressure fields, we use the two-layer PBL model of Brown and Liu (1982) that relates the geostrophic wind vector to the surface wind vector, surface roughness, humidity, stratification and thermal wind. The model includes a surface layer and an outer layer. The velocity in the surface layer increases logarithmically with height and is corrected for variable stratification using the Businger-Dyer model (Paulson 1970). The outer layer extends from the top of the surface layer to the top of the boundary layer where the flow is assumed to be in geostrophic balance. The classical Ekman spiral is

unstable to infinitesimal disturbances, so it is modified by the addition of secondary flow as proposed by Brown (1970, 1972). The flows at the interface of the surface layer and the outer layer are patched by matching velocities and the vertical shear of velocity there to relate Ekman and surface layer flow to the geostrophic wind. Kondo's (1975) empirical method which considers the flow to be laminar at very low wind speeds or small roughness, is used to obtain the roughness length from the winds through the friction velocity. Molecular effects in the interracial layer mentioned by Liu et al. (1979) are also considered.

The basic equations are:

In the Ekman/Taylor layer,  $U$  and  $V$  can be expressed as:

$$\begin{aligned} U &= \cos \alpha + u_t \zeta - e^{-\zeta} [(\cos \zeta - \sin \zeta) \sin \alpha + v_t \cos \zeta] + U_2 \\ V &= -\sin \alpha + v_t \zeta + e^{-\zeta} [(\cos \zeta - \sin \zeta) \sin \alpha + v_t \sin \zeta] + V_2 \end{aligned} \quad (1)$$

where  $u_t$  and  $v_t$  are the zonal and meridional components of the thermal winds,  $U_2$  and  $V_2$  are secondary flow, and  $a$  is the geostrophic departure angle, the lower boundary condition is the wind at the top of the surface layer. The direction of  $U$  is defined as the direction of the surface wind.  $V$  is the wind perpendicular to the surface wind at any level.  $\zeta \equiv z/L$  is the non-dimensional stability function and  $L$  is the Monin-Obukhov length. The effect of moisture fluctuations on buoyancy is included in  $L$ .

In the surface layer, the logarithmic profile is used:

$$U_s / u_* = 1/k [\ln(z/z_0) - \psi(z/L)] \quad (2)$$

Here  $U_s$  is the surface wind (measured by the scatterometer in our case),  $u_*$  is the surface wind stress,  $z$  is the height of wind speed measurement,  $Z_0$  is the surface roughness length,  $k$  is von kármán's constant, and  $\psi$  is a function of  $\zeta \equiv z/L$ .

Then we match the solutions of the two layers at the top of the surface layer (which is assumed to be the height where scatterometer winds are measured, which is 19.5 m) to obtain the following matching conditions (Brown, 1981):

$$\begin{aligned}
B &= (1 - \lambda \psi(HL)) e^\lambda / (2\lambda \cos \lambda) \\
A' &= -\ln(\lambda E_0) + \psi(HL) - (\cos \lambda - \sin \lambda) B / e^\lambda \\
E &= \delta / z_0 = 2k\lambda u_* / [fz_0(1 - \lambda \psi_\zeta(HL))] \\
\beta &= e^\lambda / 2 \cos \lambda [-u_t(\lambda) + (\cos \lambda + \sin \lambda) v_t / e^\lambda - U_2(\lambda)] \\
\gamma &= \lambda u_t(\lambda) + \cos \lambda v_t / e^\lambda + U_2(\lambda) - (\cos \lambda - \sin \lambda) \beta / e^\lambda \\
HL &= \lambda \delta / L, \text{ and } \delta = 2ku_*\lambda / [f(1 - \lambda \psi_\zeta)]
\end{aligned} \tag{3}$$

Stratification, thermal wind and humidity effects can be added to the neutrally stratified profile if air-sea temperature difference and humidity are known. For our problem, only  $U_S$  is known and ECMWF air-sea temperatures are used. We can first employ Kondo's (1975) method for obtaining CD'S and  $z_0$  in different ranges of  $U_S$ 's.  $u_*$  can be obtained by an iterative method considering stratification given in the term  $z/L$ . Since  $L$  and  $Z$  are also functions of  $u_*$ , further iteration is required.

At this point, we can use matching conditions to solve for the turning angle  $a$  and  $G$  (geostrophic wind), since the similarity parameters  $B$  and  $A'$  can be obtained if we know  $\lambda$ ,  $u$ ,  $v_t$ ,  $U_2$  and  $V_2$ .  $\lambda$  is the ratio of the height of the surface to the outer layer characteristic scale,  $\delta$ . It is found to be approximately 0.15 (Brown 1978).

After  $G$  and  $a$  are determined, horizontal pressure gradients can be obtained from the geostrophic relations. Thus, as long as we know boundary conditions, the pressure field can be computed through surface winds using this boundary layer model.

In summary, we first obtain roughness length  $z_0$  and frictional velocity  $u_*$  by iteration from the observed surface velocity, using the method of Kondo (1975). Then we determine the turning angle and magnitude of the geostrophic wind from the matching

conditions. Finally, we use the **geostrophic** wind vectors to construct the surface pressure field through the **geostrophic** relations. An inversion method (Wunsch, 1978) is used to reduce errors during integration.

It has been known for many years (e.g., Webb 1970) that models of the PBL based on the log-linear profile **are** deficient **in** their representation of the flow under conditions of strong stability. **An** alternative procedure is the one suggested by Webb (1970), who uses a modified **log-profile** under conditions of **large** stability. We found little difference in the results using **the** two procedures. **In** our **cases**, **the** wind speeds are too small to produce any significant change in **geostrophic** winds.

This model has been used in several major field experiments to derive surface wind fields from surface pressure fields to **verify** observed winds. For example, the Arctic Ice Dynamics Joint Experiment (AIDJEX) (Brown 1981), GOASEX (Woiceshyn 1979) and the Joint Air-Sea Interaction Experiment (JASIN; Brown et al. 1982). Here we invert the model to obtain pressure fields from surface winds.

Various forms of this model **have also been** used rather successfully in deriving surface pressure fields from the data gathered by scatterometer winds. Scatterometer winds were used to **reconstruct** surface pressures over limited regions during different synoptic storm situations (Brown and Levy 1986; Brown and Zeng 1994), in the southern hemisphere (Levy and Brown 1991), and for tropical cyclones by incorporating gradient wind dynamics (Hsu and Liu 1996).

Air temperature was not a parameter measured by Seasat, but the PBL model is sensitive to air-sea temperature difference as a measure of the near-surface atmospheric stratification. Thus, in keeping with the **effort** to restrict our data input to satellite observations, we have explored the effect of **arbitrarily** prescribing an air-sea temperature difference. Where the winds have a **poleward** component, we consider the air to be  $1^{\circ}\text{C}$

warmer than the sea surface, and where the winds have equatorward component, we consider the air to be 1 °C colder than the sea surface. The contribution of atmospheric stratification to the derived pressure field is discussed in detail in section 4c.

*b. Inverse Method*

. We derive pressure values from geostrophic winds and observations using an inverse method described by Wunsch (1978):

$$\mathbf{A} \mathbf{x} = \mathbf{b} \tag{4}$$

where  $\mathbf{x}$  is a column vector with unknown pressure values.  $\mathbf{A}_{ij}$  is an  $m \times n$  matrix with elements equal to the points with latitude index  $i$  and longitude index  $j$ .  $n$  is equivalent to the total grid points considered. The rows of  $\mathbf{A}_{ij}$  contain zeroes everywhere except for the elements corresponding, to the points that are used in the finite difference scheme used to represent the pressure gradient at the point  $j$  in the  $\mathbf{b}$  matrix.  $\mathbf{b}$  is a  $n$ -dimensional column vector that contains the pressure gradients. Pressure values at each point can be determined by adding a constraint on the mean pressure level from the observations. Both  $\mathbf{A}$  and  $\mathbf{b}$  are inexact. Any solution will be an estimate,  $\hat{\mathbf{x}}$ , of the true  $\mathbf{x}$ . The matrix  $\mathbf{A}$  can be inverted by singular value decomposition (SVD), where

$$\mathbf{A} = \mathbf{V} \mathbf{\Lambda} \mathbf{U}^T \tag{5}$$

the superscript T denotes the transpose of a matrix  $\mathbf{A}$  and  $\mathbf{\Lambda}$  is a diagonal matrix with elements equal to eigenvalues. The system can be solved by

$$\hat{\mathbf{x}} = \mathbf{V} \mathbf{\Lambda}^{-1} \mathbf{U}^T \mathbf{b} \tag{6}$$

to obtain the pressure field with least square errors.

## 4. Results

### *a. PBL-model-derived pressure fields and comparison with NCEP analyses and ECMWF analyses*

The PBL-model-derived pressure field (hereafter PSASS) over the North Pacific, extending from  $155^{\circ}\text{E}$  to  $135^{\circ}\text{W}$  and  $20^{\circ}\text{N}$  to  $55^{\circ}\text{N}$ , at 1200 UTC on 11 September 1978 is shown in Fig. 2a. There are two primary low centers in the northern part of the domain and one high center in the eastern subtropical Pacific. For comparison, we show in Figs. 3a and 4a the operational surface pressure analyses for 1200 UTC on 11 September 1978 produced at the U. S. National Centers for Environmental Prediction (NCEP; Fig. 3a) and the European Centre for Medium Range Weather Forecasting (ECMWF; Fig. 4a). The patterns in these three fields (pSASS, NCEP and ECMWF) are broadly similar.

Looking at the fields in more detail, we see that in the PSASS field, the low in the northwestern Pacific is located at  $166^{\circ}\text{E}$ ,  $47^{\circ}\text{N}$  and has a central pressure of 990 mb. A second cyclonic center is located in the Gulf of Alaska near  $151^{\circ}\text{W}$ ,  $49^{\circ}\text{N}$  and has a central pressure of 987 mb. The subtropical high in the eastern Pacific has a central pressure of 1024 mb and is located slightly east of an anticyclonic center in the wind field.

The NCEP analysis also shows two low centers, one near  $167^{\circ}\text{E}$ ,  $47^{\circ}\text{N}$ , the other near  $152^{\circ}\text{W}$ ,  $50^{\circ}\text{N}$ . The low center in the derived pressure field in the northwestern part of the domain is located about 1 degree west of the corresponding NCEP analyzed low and has a central pressure 2 mb higher than that in the NCEP analysis (988 mb). The other low center is 5 mb lower than that in the NCEP analysis and is located about  $2^{\circ}$  west and  $1^{\circ}$  south of the low in the NCEP analysis. The position of the derived subtropical high center in the eastern Pacific is nearly identical to that in the ECMWF analysis and is 2 mb lower than that in the NCEP analysis (1026 mb).

The two lows in the **ECMWF** analysis are located near  $169^{\circ}\text{E}$ ,  $47^{\circ}\text{N}$  and  $151^{\circ}\text{W}$ ,  $50^{\circ}\text{N}$ . The central pressures are 989 mb and 991 mb. The position of the subtropical high is close to that in both the NCEP and PSASS fields, while it has a central pressure of 1024 mb, which is exactly the same as that in PSASS. The pattern of the derived low in the eastern part of the domain bears a closer resemblance to that in the **ECMWF** analysis.

Six hours later, at 1800 UTC, *the* PSASS **primary** low center in the northwestern Pacific has moved about 6 degrees east to  $172^{\circ}\text{E}$ ,  $46^{\circ}\text{N}$  (Fig. 2b), while the NCEP analyzed low has only moved slightly east to  $170^{\circ}\text{E}$ ,  $47^{\circ}\text{N}$  (Fig. 3b). In the **ECMWF** analysis (Fig. 4b), the position of this low is closer to that in the **PSASS** field. Its central pressure is now 991 mb in the **PSASS** field, which is 5 mb higher than that in the NCEP analysis and 4 mb higher than that in the ECMWF analysis. Again, we can see that our PSASS field resembles the ECMWF pressure field slightly more. The principal low in the Gulf of Alaska, according to the NCEP analysis, is near  $152^{\circ}\text{W}$ ,  $50^{\circ}\text{N}$  with a central pressure of 984 mb, while in our derived pressure field, it is located at  $151^{\circ}\text{W}$ ,  $51.5^{\circ}\text{N}$  with a central pressure of 979 mb. When we examine the cyclonic centers of the high density wind barbs we find that the low centers are very close to these cyclonic centers. For the NCEP analyses, there are no observations near the center of the lows plotted in their surface analyses. Therefore, we strongly favor our derived pressure fields for locating low centers. The position and central pressure of the subtropical high in the eastern Pacific is close to that in the NCEP analysis. However, the subtropical high in the **ECMWF** analysis is about 3 degrees east and the central pressure is 1 mb lower than both NCEP analysis and PSASS field.

A second case, that of 1800 UTC, 14 September 1978, showing a belt of high pressure over the northern Pacific ocean, is shown in Figs. 2c, 3c and 4c. In the NCEP analysis (Fig. 3c), the trailing end of a cold front in the northeastern part of the domain

separates two high centers with the same central pressure of 1030 mb. A third high center is located in the western Pacific at  $165^{\circ}\text{E}$ ,  $44^{\circ}\text{N}$  with a central pressure of 1029 mb.

The PBL-derived pressure field shows this belt of **highs** (Fig. 2c). **There** is general agreement between **the** derived pressure field and the NCEP and the ECMWF analysis. The major discrepancy is a low that appears at  $139^{\circ}\text{W}$ ,  $36^{\circ}\text{N}$ . Our analysis shows a trough between the high centers, whereas the NCEP analysis exhibits a continuous belt of high pressure. Unlike the NCEP analysis, the **ECMWF** analyzed pressure field **also** shows a local trough near the this region, except **the** position is further north of that in the derived field.

Even though the **highs** are similar both in magnitudes and features in most region for PBL derived field, NCEP and ECMWF fields, there is one exception -- the PSASS derived high in the western Pacific is stronger than that in both the NCEP analysis and the ECMWF analysis. There is no observational evidence to support, pressures in this region as **high** as 1036 mb. ECMWF has 1031 mb (Fig. 4c) and NCEP has 1029 mb (Fig. 3c). **This PSASS** central pressure is presumably due to the strong winds south of  $40^{\circ}\text{N}$  and north of  $45^{\circ}\text{N}$ , with speeds of 15 to 20  $\text{m s}^{-1}$  (not shown). As an alternative hypothesis, we considered that anomalous high pressure gradient might be due to a thermal wind effect, but introducing this (from ECMWF surface temperature fields) into the PBL model produced no appreciable difference in the pressure field. This absence of thermal wind influence is consistent with the results reported by Brown and Levy (1986), who remark that in the presence of strong winds and stable flow, the boundary layer is too shallow to allow baroclinic influence. (See also Levy and Tiu 1990, who emphasize the greater effect of stratification in comparison with the thermal wind and note that the effect of thermal wind is mainly on the turning angle rather than the magnitude of the geostrophic wind). A summary of the positions and central pressures are given in Table 1.

Table 1. Comparison of position and central pressure for different analyses

case	analyses	position	central pressure
1	PSASS	166°E, 47°N	990 mb
	NCEP	167°E, 47°N	988 mb
	ECMWF	169°E, 47°N	989 mb
2	PSASS	151°W, 49°N	987 mb
	NCEP	152°W, 50°N	992 mb
	ECMWF	151°W, 50°N	991 mb
3	PSASS	139°W, 34°N	1024 mb
	NCEP	138°W, 34°N	1026 mb
	ECMWF	137°W, 34°N	1024 mb
4	PSASS	172°E, 46°N	991 mb
	NCEP	170°E, 47°N	986 mb
	ECMWF	172°E, 46°N	987 mb
5	PSASS	151°W, 51.5°N	979 mb
	NCEP	152°W, 50°N	984 mb
	ECMWF	151°W, 52°N	984 mb
	GOASEX	151°W, 52°N	980 mb
6	PSASS	136.5°W, 36°N	1026 mb
	NCEP	137°W, 35°N	1026 mb
	ECMWF	134°W, 39°N	1025 mb

## 5. Comparison with GOASEX, ship and buoy data and stratification effect

### *a Comparison with GOASEX*

Another dataset available for comparison with our derived pressure field in a region limited to the northeast Pacific are the special analyses of the GOASEX experiment in the Gulf of Alaska. The pressure field at 1800 UTC, 11 September was reanalyzed for a region near the low center in the Gulf of Alaska using GOASEX data (Fig 5). The reanalyzed low center is 980 mb. This is closer to the central pressure of that in our derived pressure field, which is 979 mb, than the 984 mb value in the NCEP analysis and

ECMWF analysis. The location of this low is 151 °W, 52°N in the GOASEX reanalysis, which is very close to that in our SASS wind derived pressure field.

A reanalysis of the pressure field by Woiceshyn (1979) at 1800 UTC on 14 September (Fig. 6) using the GOASEX observed data shows a low near 140°W and 38°N, consistent with our derived pressure pattern. The central pressure of the GOASEX analyzed low is 1026 mb, which is precisely what we obtain in the PBL-model-derived pressure field. A comma-like cloud is near the low center in the model derived pressure field on a visible satellite image of the eastern Pacific at that time (Fig. 7).

*b. Comparison with surface buoy and ship observations*

During the Gulf of Alaska Experiment, special spot observations were made by the NOAA buoys, ocean station PAPA, and the NOAA ship Oceanographer. Data were recorded coincident with the satellite's passage and represent the most accurate estimates of the true surface conditions at the time of SeaSat measurements. Locations of NDBO (National Data Buoy Office) buoys and ships in the Gulf of Alaska are given in Table 2.

Observed surface pressure measurements from these buoy and ship observations are compared with the values at the corresponding locations and time (nearest available) obtained from the analyses from the PBL model, NCEP analysis and ECMWF analysis. From Table 3, we can see that there is broad agreement between the values obtained from the different sources. The differences vary from 0 to 4 mb for single points. The mean differences for all the cases are less or equal to 2 mb. The NCEP analyses show the smallest differences from the buoy and ship observations. For the PBL-derived fields, only one surface observation (at 20°N, 151°W) is included and it is far away from this region. Moreover, some uncertainties may be caused by the interpolation of the wind fields. Considering these factors, the performance of the PBL-derived analyses is quite satisfactory. Though the inclusion of more surface observations into the PBL analyses

will improve the **results**, our **main** objective is to use **as** few other resources **as** possible to speed up and simplify the calculation.

When we compare the analyses with weather station observations near the low center at 1800 UTC 11 September, 1978 (see Table 4), we find that NCEP analyses still performs the best and **ECMWF** analyses are slightly inferior to the others. The errors vary from 0 to 5 mb and the mean **errors** have increased slightly and vary from 2.0 mb (**NCEP** analyses) to 2.6 mb (**ECMWF** analyses). Even though the PBL model generated pressure fields seem to capture the **minimum** pressure of the low (980 mb), the position of the minimum is slightly west of that in Fig. 5, which included the observations from the **weather** stations listed in Table 4.

Table 2 Position of buoys and ships used for Table 3

Buoy/ship	ID	Location	time(date)
46002		42 30N 13000W	
46005		4600N 131 00W	
Papa		49 59N 14446W	1841 (11 Sept)
Papa		49 59N 145 23W	1854 (14 Sept)
Oceanographer		4840N 136 57W	0858 (11 Sept)
Oceanographer		48 42N 138 00W	1714 (14 Sept)

Table 3 Comparison of sea level pressure from different analyses with buoy observations for the 3 cases studied

buoy/ship ID	time(date)	Buoy/ship ID	PBL	NCEP	ECMWF
46002	1200(9/1 1)	1020.0	1021.0(1)	1019.0(1)	1019.0(1)
46005	1200(9/1 1)	1016.0	1015.0(1)	1018.0(2)	1017.0(1)
Oceanographer	0858(9/1 1)	1013.0	1013.0(0)	1014.5(1.5)	1016.0(3)
46002	1800(9/1 1)	1020.0	1021.0(1)	1022.0(2)	1022.0(2)
46005	1800(9/1 1)	1019.0	1018.0(1)	1021.0(2)	1021.0(2)
Papa	1841(9/11)	994.0	997.0(3)	995.0(1)	991.0(3)
46002	1800(9/14)	1024.0	1024.0(0)	1023.0(1)	1026.0(2)
46005	1800(9/14)	1020.0	1016.0(4)	1020.0(0)	<b>1021.5(1.5)</b>
Papa	1854(9/14)	1015.0	1012.0(3)	1013.0(0)	1014.0(1)
Oceanographer	1714(9/14)	1016.0	1014.0(2)	1015.5(0.5)	1017.5(1.5)
Mean difference from buoy			1.6	1.5	2.0

\* Numbers inside the parentheses are absolute values of the differences from buoy/ship observations

\* **Mean error is obtained by averaging the accumulated differences**

Table 4 Comparison of sea level pressure from different analyses with buoy observations for 1800 UTC, 18 Sept, 1978

position	weather ship	PBL	NCEP	ECMWF
51.5N, 151.0W	980.0	984.0(4)	985.0(5)	985.0(5)
50. ON, 152.0W	982.0	983.0(1)	984.0(2)	987.0(5)
50. ON; 154.0W	986.0	984.0(2)	984.0(2)	989.0(3)
48. ON, 149.5W	989.0	989.0(0)	993.0(4)	<b>992.0(3)</b>
54. ON, 155.0W	994.0	993.0(1)	993.0(1)	996.0(2)
50. ON, 145.0W	994.0	997.0(3)	995.0(1)	991.0(3)
48.5N, 140.0W	1008.0	1011.0(3)	1007.0(1)	1008.0(0)
50. ON, 138.5W	1008.0	1013.0(5)	1010.0(2)	1009.0(1)
40. ON, 150.5W	1009.0	1010.0(1)	1010.0(1)	1011.0(2)
37.5N, 154.0W	1013.0	1011.0(2)	1012.0(1)	1015.0(2)
mean difference		2.3	2.0	2.6

*c. Stratification effect*

Without question the stratification of the atmosphere is quantitatively significant in the derivation of pressure fields from wind fields. We have made control runs for each of our cases using neutral stratification instead of the arbitrary one-degree air-sea temperature difference as described above. The effect is not difficult to anticipate. For unstable stratification there is an increase in the downward momentum transfer and therefore in the sea-surface roughness. Thus, inverse reasoning from a given 19.5-m wind speed would infer a weaker pressure gradient when the atmosphere is unstable and a stronger gradient when it is stable.

The question we posed for ourselves was whether it is possible to formulate a simple rule for assessing a stability that would present an improvement in results over an assumption of neutrality everywhere. The answer appears to be affirmative. The neutral

runs referred to are uniformly less satisfactory in their agreement with the weather **service** analyses than the counterparts with the estimated temperature difference assigned. On 11th September, 1800 UTC, the Aleutian low center is insufficiently developed in the neutral run (Fig. 8b), with a central pressure of 987 mb. The one degree assigned temperature difference in the strong stable southerly current strengthens the gradient and results in a low of 979, about 5 mb lower than the weather service values, and one millibar lower than the GOASEX analysis. It is entirely possible that the temperature difference is greater than this, but if a 2-degree difference is assigned to southerly winds, the effect is to deepen the Aleutian center only slightly more to 978 mb.

The careful GOASEX reanalysis revealed a maximum of 3°C air-sea temperature difference in the Gulf of Alaska, but if this difference is applied to all southerly winds, the accumulated effect of the southerly flow north of 35°N is so **great** as to over-deepen the low center to 977 mb.

Thus although stratification is important in the deviation of pressure fields from wind fields, and air-sea **temperaturre** difference is not a quantity available directly from remote sensing, it does appear that even a very simple-minded algorithm can provide **an** assessment of its effect that is practically useful.

Fig. 9 shows the magnitudes of geostrophic wind versus surface winds under different stratification. Under unstable condition, the **geostrophic** wind is not sensitive to the increase of surface wind speed. It tends to decrease the **geostrophic** wind slightly through mixing with lower level winds that carry lower momentum. On the other hand, under stable condition, the **geostrophic** wind is **smaller** than the neutral case when winds are smaller than 5 m/s. However, when wind speeds exceed 5m/s, the stable stratification starts to increase the **geostrophic** wind tremendously. This effect can be seen very clearly near cyclones. Near the stable (east part in the Nor[hem Hemisphere) side of a cyclone,

isobars **can be** a lot denser than the **other** side of the cyclone. As a result, isobars around cyclones are not **symmetric**. This phenomena **can also** be seen in the **NMC** or **ECMWF** analyses.

When secondary flow effect is included (not shown), the pressure gradients always **decrease** slightly. Central pressures are within 1 or 2 mb of the neutral case with this effect considered.

## 6. **Balanced pressure**

With this **high** resolution dataset, one **might** be curious whether we can do just as well using some **other** scheme **with** simpler physics to derive pressure fields. One method of constructing pressure fields entirely from surface winds is by balancing the rotational **part** of the wind and pressure as done by **Endlich** et al. (1981).

Any velocity **field** can be **partitioned** into a nondivergent part plus an **irrotational** part such that

$$V = V_{\psi} + V_e \quad (7)$$

where

$$\nabla \cdot V_{\psi} = 0 \text{ and } \nabla \times V_e = 0 \quad (8)$$

For **midlatitude** synoptic scale motions  $V$  is quasi-nondivergent according to scale analysis of the vorticity equation (**Holton** 1979). The remaining terms in the **vorticity** equation, when divergent winds **are neglected**, imply a relationship of nondivergent winds to the height (pressure) fields which is the well known balance equation. It can be written as

$$g\nabla^2 Z = f\zeta - \beta u + 2J(u, v) \quad (9)$$

where  $Z$  is the height of a pressure surface,  $f$  is the coriolis parameter,  $\zeta$  is the relative vorticity,  $\beta = \partial f / \partial y$ , and  $J(u, v) = (\partial u / \partial x)(\partial v / \partial y) - (\partial u / \partial y)(\partial v / \partial x)$ .

To obtain height (pressure) fields from the balance equation, pressures at all boundary points are required when solving the Poisson equation. The computed height fields are converted to pressure fields through the hydrostatic relation. A successive relaxation scheme was applied to solve the equation after the boundary values were prescribed. Pressure values at boundaries are taken from the NCEP analyses. For all the cases calculated, the pressure values were found to converge very rapidly.

To divide the winds into the rotational and divergent parts, the method of direct vector alterations (Endlich, 1967) are used. The desired wind fields are obtained by a point iterative method applied to the two simultaneous linear partial differential equations that define horizontal divergence and relative vorticity. The divergent vectors are believed to be a lot smaller than the nondivergent vectors. For the cases we studied, however, the divergent winds are usually of comparable magnitudes with the nondivergent winds and are not negligible near the low centers.

We have applied this technique to derive the balanced pressure fields for the 3 cases examined above. Fig. 9a shows the balanced pressure field for 1200 UTC on 11 September 1978. We can see that the balanced pressure field is much smoother and has less structure than either the NCEP (Fig. 3a), ECMWF (Fig. 4a) or PSASS fields (Fig. 2a). Even very near the northern boundary, where we have the same boundary values as those in the NCEP field, the primary low center near the northwestern Pacific has a central pressure of 995 mb. This is 9 mb higher than that in the NMC analysis and 5 mb higher than that in our PBL-derived pressure field with a 1 °C air-sea temperature difference imposed. The primary low in the eastern Pacific has a central pressure of about

994 mb, which is 7 mb higher than that in the PSASS analysis. The position of the low center in the northwestern pacific is close to that in the NCEP analysis (note that the domain only extends to 50°N in the balanced pressure field), while the low center in the Gulf of Alaska is 2 degrees west of that in the NCEP analysis. Even worse is the position of the subtropical high, which is about 10 degree east of the high in the NCEP analysis, and is also much weaker.

The pressure gradients are underestimated in the balanced-pressure fields; therefore, the central pressures are usually higher in the lows and lower in the highs (compared with Figs. 2). This can be seen most clearly in the pressure difference chart (Figs. 11), obtained by subtracting balanced pressures from PBL-model-derived pressures. The most prominent differences appear at high and low centers where divergence is largest. These differences can be as large as 10 mb. A region of low values in the difference chart near 165°W, 42°N is mainly due to the failure of the balanced pressure field to capture the position and strength of the low center in that region.

We have made extensive computations of the divergence and vorticity values from the SASS winds and found that although divergence is generally smaller than vorticity, the values are of the same order of magnitude. Endlich et al. (1981) attribute the discrepancies in their derived pressure fields to the asynoptic nature of their wind data. From our synoptic analysis, we can see that the difference is systematic. Therefore, we conclude that the errors in the balanced-pressure fields are chiefly due to the neglect of divergence.

## 7. Conclusions

The construction of detailed synoptic marine surface pressure fields from surface winds alone, **measured** by satellite, **has** been achieved. The pressure fields are obtained from SASS winds through a two-layer marine PBL model that includes **ageostrophic** winds produced by secondary **flow**, stratification, thermal wind and **humidity**. **It should be** noted that our results are subject to limitations by the boundary layer model used, **notably**, the assumption of the **geostrophic** balance of the wind and pressure fields at the top of the boundary layer fields. **These PBL-model-derived** pressures are compared with NCEP and **ECMWF** analyses **and** special analyses based on data gathered by GOASEX. Balanced-pressure **fields** are also obtained as references for comparison. **We** can conclude the **following**:

1. Pressure fields derived from SASS winds using a two-layer PBL model are of a quality comparable to **those** of the NCEP and **ECMWF** analyses in the north pacific that were produced in 1978.
2. Balanced pressure **fields** are systematically inferior to those derived using a two-layer PBL model.
3. **PBL-model-derived** pressure fields can detect **mesoscale** features not resolved in the weather service **analyses**.
4. The SASS-derived pressure fields **are** as close to the NCEP and **ECMWF** fields in pattern and central pressures as these two **are** close to each other.
5. Central pressures, especially those in low centers, are highly sensitive to stratification due to the **strong northerly** and southernly currents surrounding them. Even without **observational** evidence of the air-sea **temperature** difference, the assumption of a plus-or-minus one **degree** difference, according as the flow is toward the north or south, produces a marked improvement over the assumption of a neutral atmosphere, as **judged** by agreement with conventional analyses.

6. Atmospheric stratification tends to intensify low centers and suppress high centers. The effect is most prominent near the stable side of cyclones where wind speeds are strong. Inclusion of atmospheric stratification in the calculation yields more accurate results.

The successful derivation of pressure fields from scatterometer wind fields is significant in two respects. First, the accuracy of these fields will be increased in areas of sparse data. Second, fields derived from scatterometer data alone can be available without the delay occasioned by the data processing and assimilation in forecasting centers. This should be of great value in short-range forecasting or now-casting. Even with the launch of ERS-1, the data is single swath and separations between swaths are large and there is not enough coverage to derive synoptic pressure fields, especially near fast developing storms as the cases we demonstrated. The recent launch of NASA scatterometer (NSCAT) on ADEOS 1 (Advanced Earth Observing Satellite) in August, 1996 and the scheduled launch of SeaWinds scatterometer on ADEOS2 in 1999 with better coverage give us the promise of advancing our investigations.

## Acknowledgments

The authors greatly acknowledge Dr. R A. Brown of the University of Washington for his insightful discussions on the PBL model. We are also grateful to Dr. Ichiro Fukumori for his stimulating discussions on the inverse methods. Comments from three anonymous reviewers are very much appreciated. Encouragement and support from Dr. Don Collins at the PO.DAAC is very much appreciated. The research described in this paper was carried out in part by the Jet propulsion Laboratory, California Institutes of Technology, under a contract with the National Aeronautics and Space Administration.

## References

- Anderson, D. A. Hollingsworth, S. Uppala, p. Woiceshyn, 1991: A study of the use of scatterometer data in the European Centre for Medium-Range Weather Forecasts Operational Analysis-Forecast Model, 2, Data Impact. *J. Geophys. Res.*, **96**, 2635-2648.
- Atlas, R., P. M. Woiceshyn, S. Peteherych and M. G. Wurtele, 1982: Analysis of satellite scatterometer data and its impact on weather forecasting. *Oceans*, 82,415-420.
- Brown, R. A., 1970: A secondary flow model for the planetary boundary layer. *J. Atmos. Sci.*, **27**,742-757.
- Brown, R. A., 1972: The inflection point instability problem for stratified rotating boundary layers. *J. Atmos. Sci.*, **29**,850-859.
- Brown, R. A., 1981: Modelling the geostrophic drag coefficient for AIDJEX. *J. Geophys. Res.*, **86**, 1989-1994.
- Brown, R. A. and G. Levy, 1986: Ocean surface pressure fields from satellite sensed winds. *Mon. Wea. Rev.*, **114**, 2197-2206.
- Brown, R. A. and T. Liu, 1982: An operational large-scale marine PBL model. *J. Appl. Meteor.*, **21**,261-269.
- Brown, R. A. and L. Zeng, 1994: Estimating central pressures of oceanic midlatitude cyclones. *J. Appl. Meteor.* **33**, 1088-1095.
- Brown, R. A., V. J. Cardone, T. Guymmer, J. Hawkins, J. E. Overland, W. J. Pierson, S. Peteherych, J. C. Wilkerson, P. M. Woiceshyn and M. G. Wurtele, 1982: Surface wind analysis for Seasat. *J. Geophys. Res.*, **87**, 3355-3364.
- Cane, M. A., and R. Atlas, 1986: The potential impact of scatterometry on oceanography: A wave forecasting case, *Oceanography from Space*, Plenum, New York, 587-595.
- Duffy D. G., and R. Atlas, 1986: The impact of SEASAT-A scatterometer data on the numerical prediction of the Queen Elizabeth II storm. *J. Geophys. Res.*, **91**, 2241-2248.

- Endlich, R. M., D. E. Wolf, C. T. Carlson and J. W. Maresca, Jr., 1981: Oceanic wind and balanced pressure-height fields derived from satellite measurements. *Mon. Wea. Res.*, **109**,2009-2016.
- Harlan, J. Jr., and J. J. O'Brien, 1986: Assimilation of scatterometer winds into pressure fields using a variational method. *J. Geophys. Res.*, **91**,7816-7836.
- Hsu, S. C. and W. T. Liu, 1996: Wind and pressure fields near tropical cyclone Oliver derived from scatterometer observations. *J. Geophys. Res.*, **101**, 17021-17027.
- Hsu, S. C., W. T. Liu and M. G. Wurtele, 1997: Impact of scatterometer winds on hydrological forcing and convective heating. *Mon. Wea. Rev.*, in press.
- Jones, W. L., L. C. Schroeder, D. H. Boggs, E. M. Bracelente, R. A. Brown, G. J. Dome, W. J. Pieson and F. J. Wentz, 1982: The Seasat-A satellite scatterometer: The geophysical evaluation of remotely sensed wind vectors over the ocean. *J. Geophys. Res.*, **87**,3297-3317.
- Kondo, J. 1975: Air-sea bulk transfer coefficients in diabatic conditions. Bound-layer *Meteo.* **9**,91-112.
- Lenzen, A. J., D. R. Johnson, and R. Atlas, 1993: Analysis of the impact of Seasat scatterometer data and horizontal resolution on GLA model simulations of the QE II storm. *Mon. Wea. Rev.*, **121**,499-521.
- Levy, G., and R. A. Brown, 1991: Southern hemisphere synoptic weather from a satellite scatterometer. *Mon. Wea. Rev.*, **119**, 2803-2813.
- Levy, G., and F. S. Tiu, 1990: Thermal advection and stratification effects on surface winds and the low level meridional mass transport. *J. Geophys. Res.*, **95**, 20,247-20257.
- Liu, W. T., K. B. Katsaros, and J. A. Businger, 1979: Bulk parameterization of air-sea exchanges of heat and water vapor including the molecular constraints at the interface. *J. Atmos. Sci.*, **36**, 1722-1735.

- McMurdie, L. A., and K. B. Katsaros, 1987: Atmospheric water distribution in a midlatitude cyclone observed by the Seasat Scanning Multichannel Microwave Radiometer. *Mon. Wea. Rev.*, **113**, 584-598.
- Overland, J. E., P. M. Woiceshyn, and M. G. Wurtele, 1980: SEASAT observations of cyclones. *Tropical Ocean-Atmosphere Newsletter*, **3**, p.7.
- Paulson, C. A., 1970: The mathematical representation of wind speed and temperature profiles in the unstable atmospheric surface layer. *J. Appl. Meteor.*, **9**, 857-886.
- Peteherych, S., M. G. Wurtele, P. M. Woiceshyn, D. H. Boggs and R. Atlas, 1984: First global analysis of SEASAT scatterometer winds and potential for meteorological research, Proceedings of the URSI commission F Symposium and Workshop, Shosh, Israel, May 14-23, NASA Conf. Publ. CP-2303, 575-585.
- Stoffelen, A. C. M. and G. J. Cats, 1991: The impact of Seasat-A scatterometer data on high-resolution analyses and forecasts: The development of the QEII storm. *Mon. Wea. Rev.*, **119**, 2794-2802.
- Webb, E. K., 1970: Profile relationships: the log-linear range, and extension to strong stability. *Quart. J. Met. Soc.*, **96**, 67-90.
- Woiceshyn, P. M., (Ed), 1979: SEASAT Gulf of Alaska Experiment Workshop, Vol. II, Comparison data base. Conventional marine meteorological and sea surface temperature analyses, Appendices A and B, Doc. 6---101, JPL, Pasadena, CA.
- Woiceshyn, P. M., M. G. Wurtele, G. F. Cunningham, 1989: Wave hindcasts forced by scatterometer and other wind fields, 2nd International Workshop on Wave Hindcasting and Forecasting, Vancouver, B. C., April 1989.
- Woiceshyn, P. M., M. G. Wurtele, D. H. Boggs, L. F. McGoldrick and S. Peteherych, 1986: The necessity for a new parameterization of an empirical model for wind/ocean scatterometry. *J. Geophys. Res.*, **91**, 2273 -2288.
- Wunsch, C., 1978: The north Atlantic general circulation west of 50°W determined by inverse methods. *Rev. Geophys. Space Phys.*, **16**, 583-620.

## Figure caption

Fig. 1. **Dealiased**, subjectively analyzed synoptic **scatterometer** wind fields (m/s) and model derived surface pressure field (rob) for 1800 UTC 11 **Sept**, 1978. Winds are reduced to one third of the original resolution. (10 by 10).

Fig. 2. PBL model derived surface pressure field from SASS synoptic **scatterometer** wind vectors with **1** °C air-sea temperature difference for 1200 UTC 11 **Sept**. 1978 (upper), 1800 UTC 11 **Sept**, 1978 (middle), and 1800 UTC 14 **Sept**, 1978 (lower).

Fig. 3. The corresponding **NMC** analysis as in Fig. 2.

Fig. 4. The corresponding **ECMWF** analysis as in Fig. 2.

Fig. **5**. Reanalyzed surface pressure field for the region near Gulf of Alaska at 1800 UTC, 11 September, 1978 (After **McMurdie** et al. 1987).

Fig. 6 Reanalysis of surface pressure field using **GOASEX** observed data at 1800 UTC on 14 **Sept**. 1978.

Fig. 7 Visible satellite cloud image for the northern Pacific at the time of Fig. 6.

Fig. 8 PBL model derived surface pressure fields as in Fig. 2, except for neutral stability.

Fig. 9 Relationship of the magnitude of surface wind versus geostrophic wind under different stratification.

Fig. 10. As in Fig. 2, except for balanced pressure fields.

Fig. 11 Pressure difference charts derived by subtracting the balanced pressure fields (Fig. 10) from the PBL model derived pressure fields (Fig. 2).

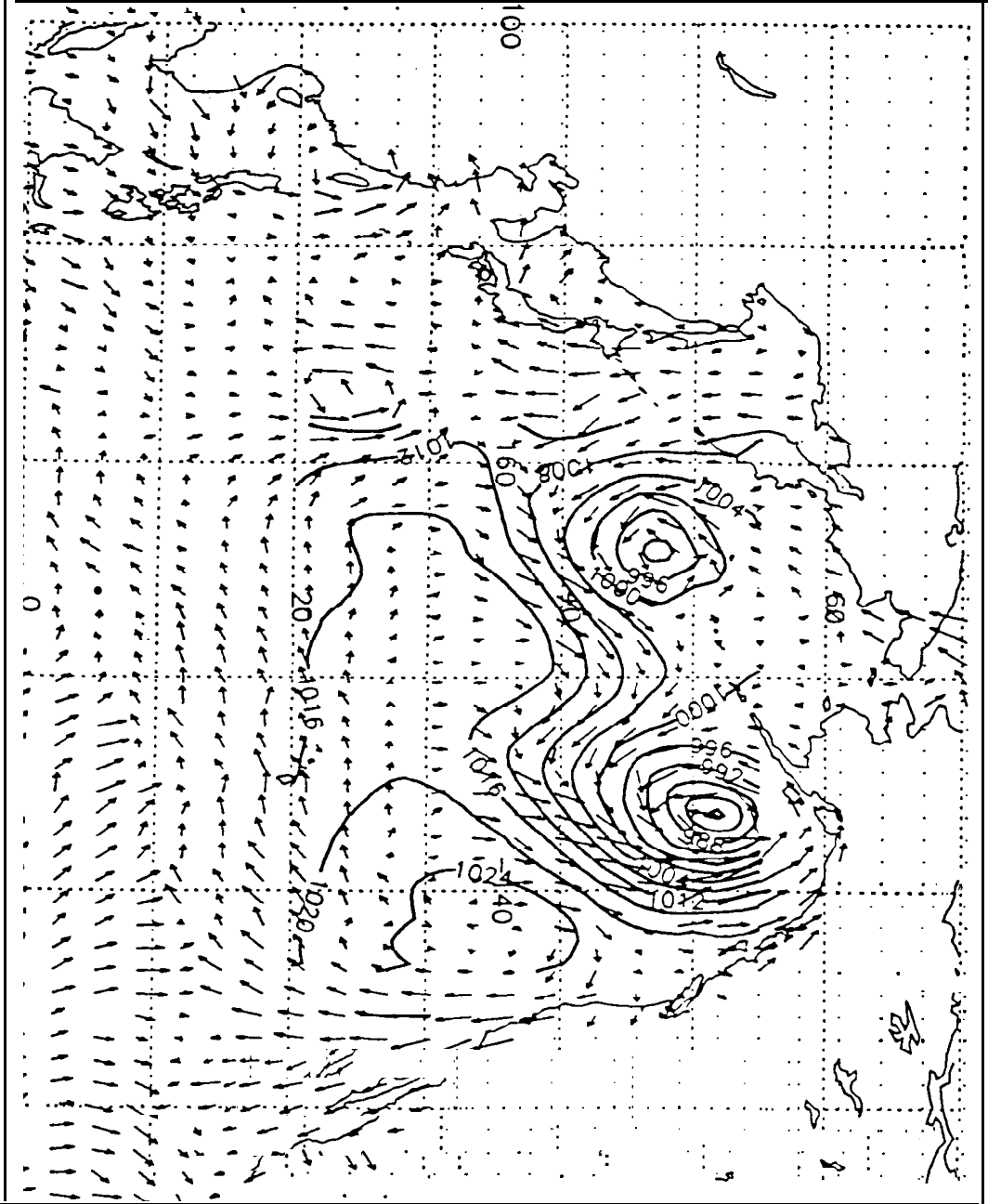
### **Table Caption**

**Table 1** Comparison of position and central pressure for different analyses.

Table 2 Position of buoys and ships used for Table 3.

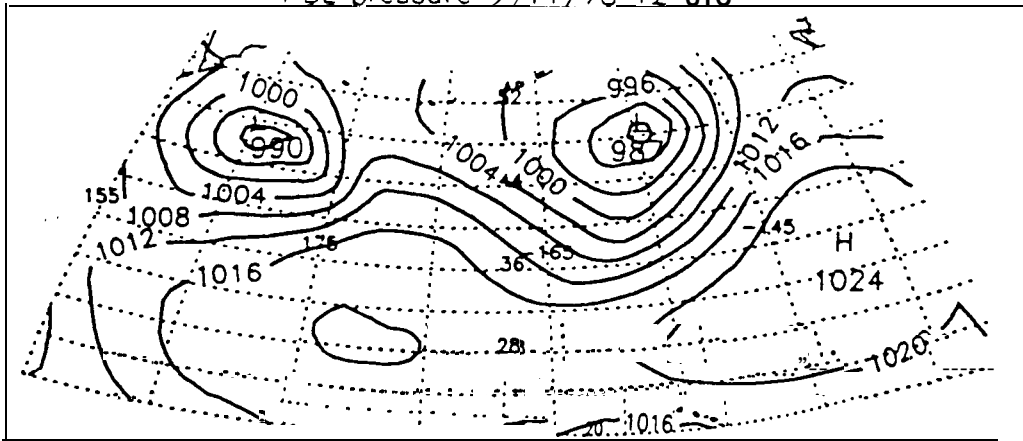
Table 3 Comparison of sea level pressure from different analyses with buoy observations for the 3 cases studied.

Table 4 Comparison of sea level pressure from different analyses with buoy observations for 1800 UTC, 18 Sept, 1978.

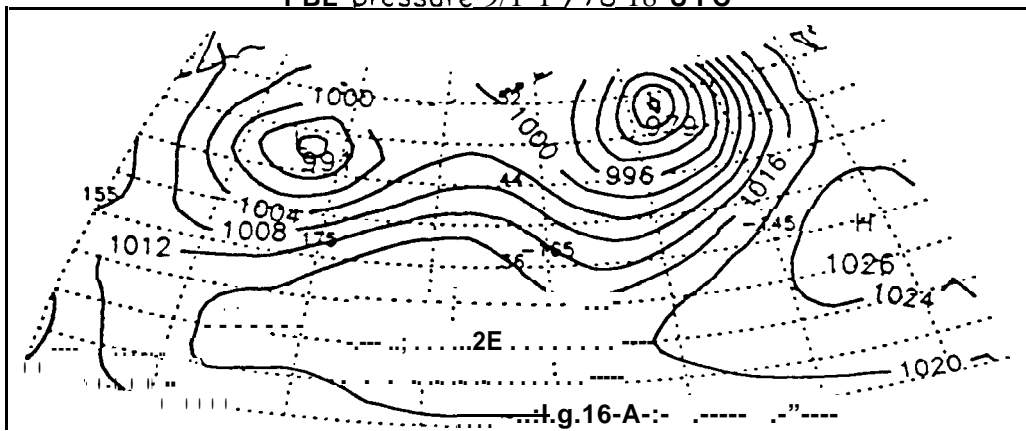


I 10 m/s

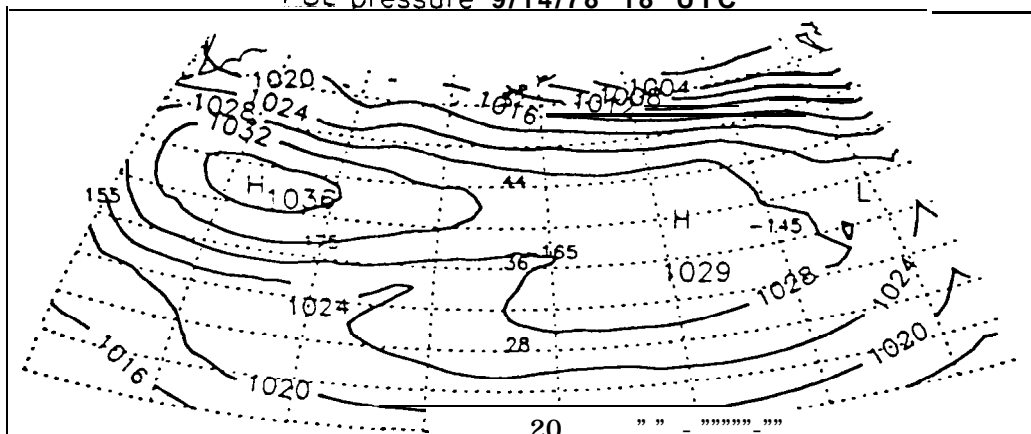
PBL pressure 9/11/78 12 UTC



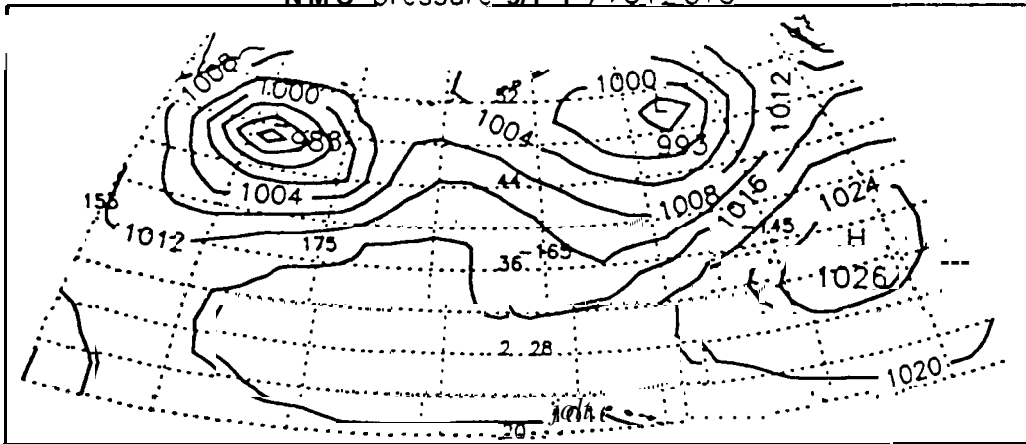
PBL pressure 9/11/78 18 UTC



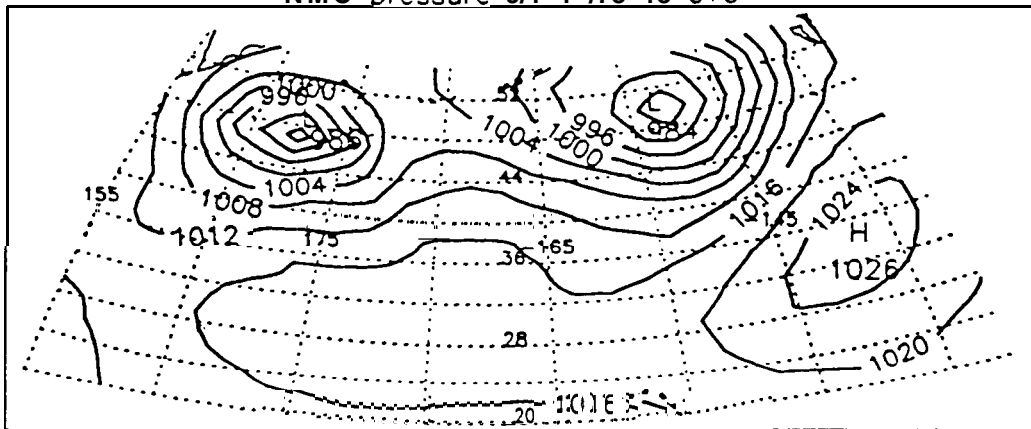
PBL pressure 9/14/78 18 UTC



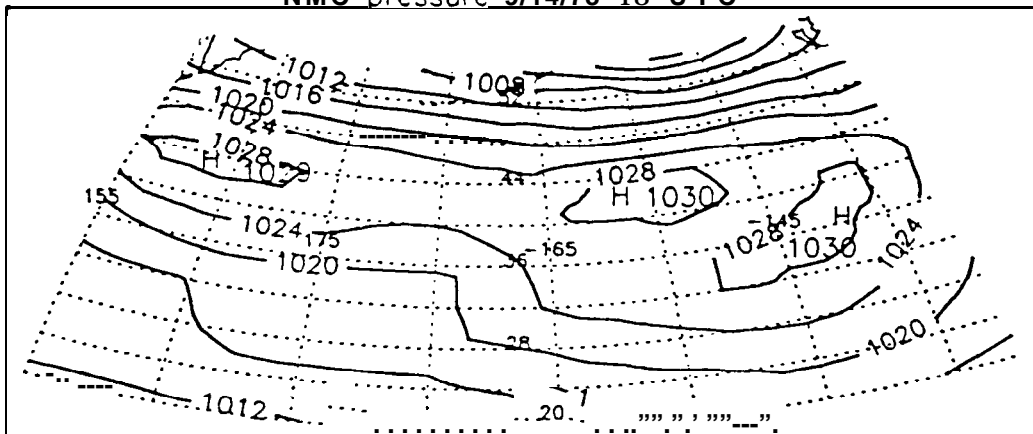
NMC pressure 9/1 1 /7812UTC



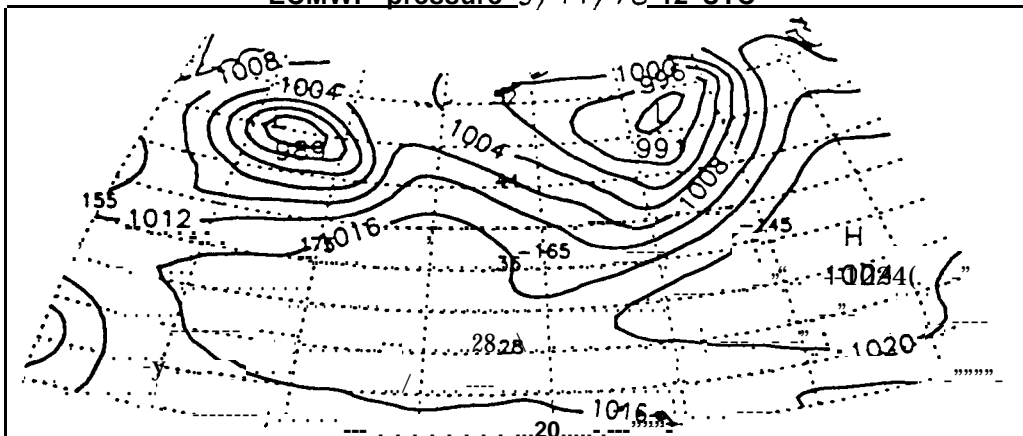
NMC pressure 9/1 1 /78 18 UTC



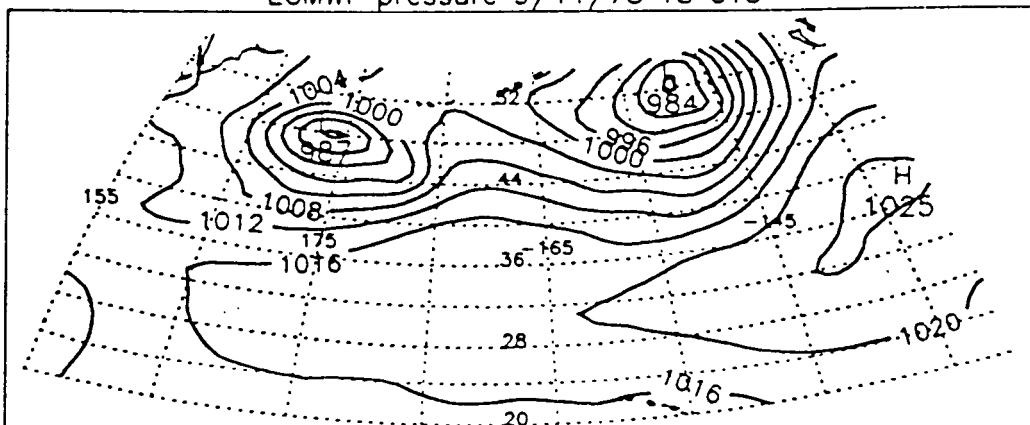
NMC pressure 9/14/78 18 UTC



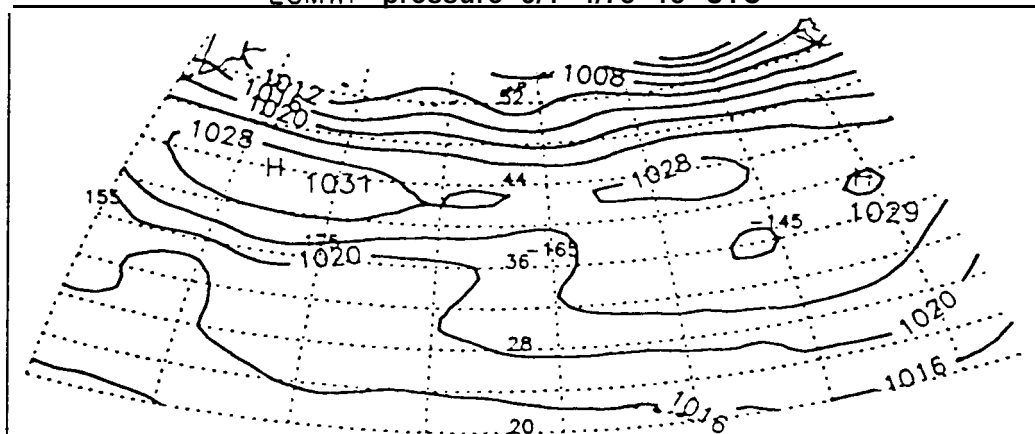
ECMWF pressure 9/11/78 12 UTC

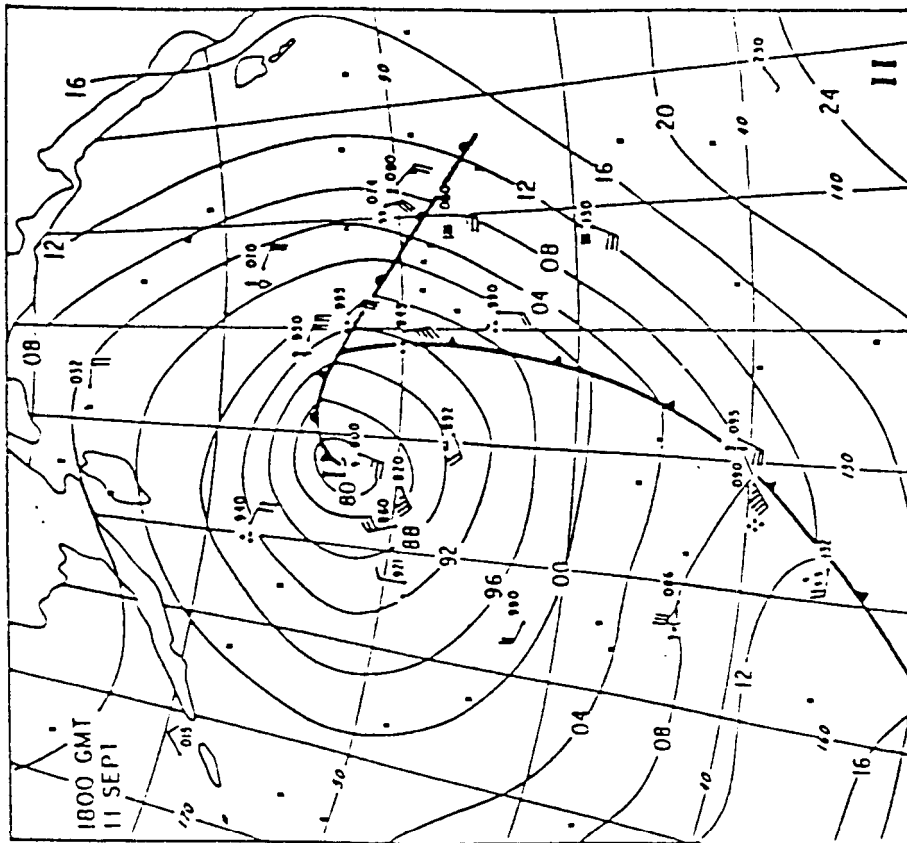


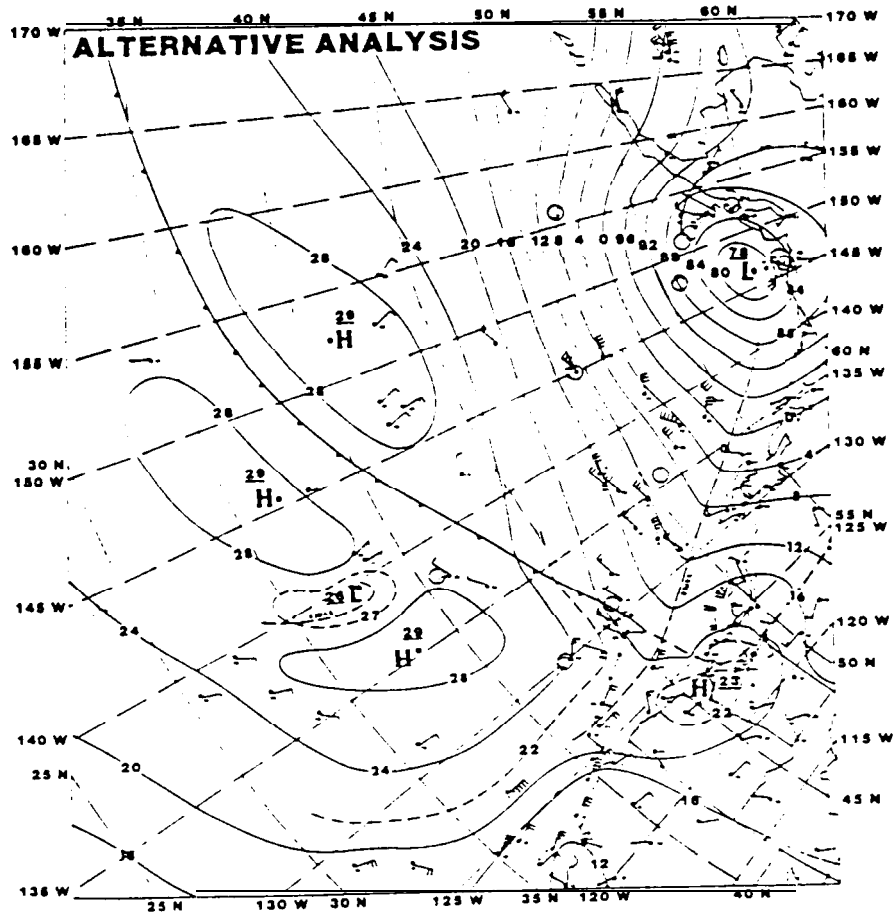
ECMWF pressure 9/11/78 18 UTC



ECMWF pressure 9/14/78 18 UTC

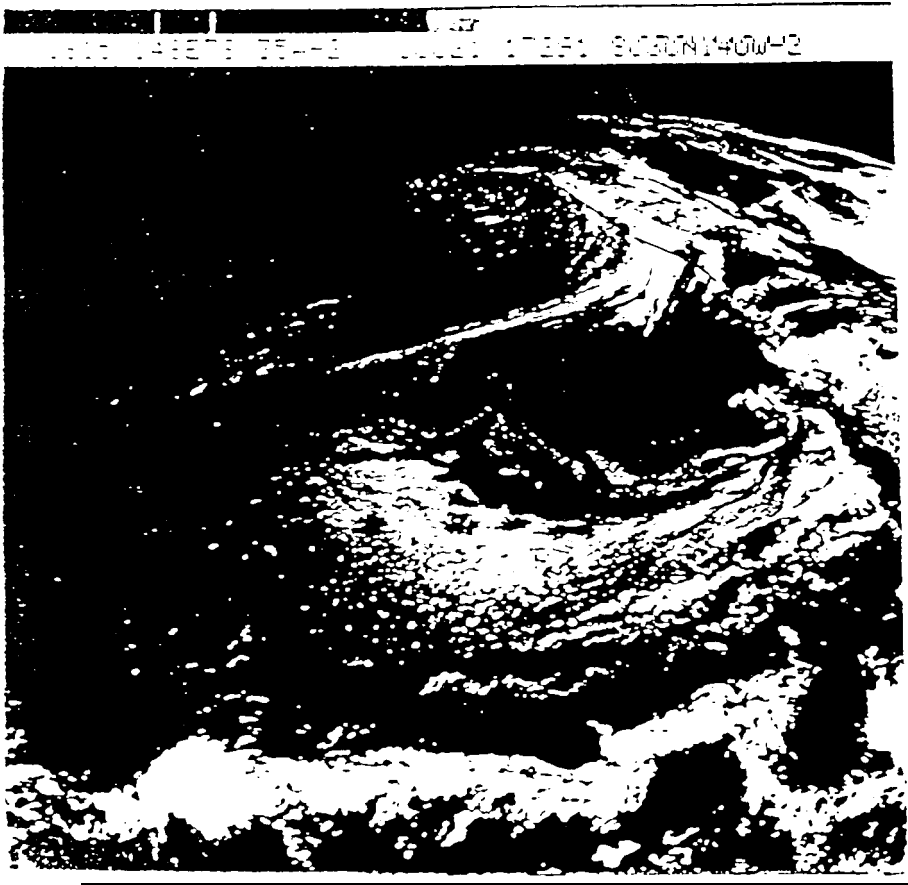




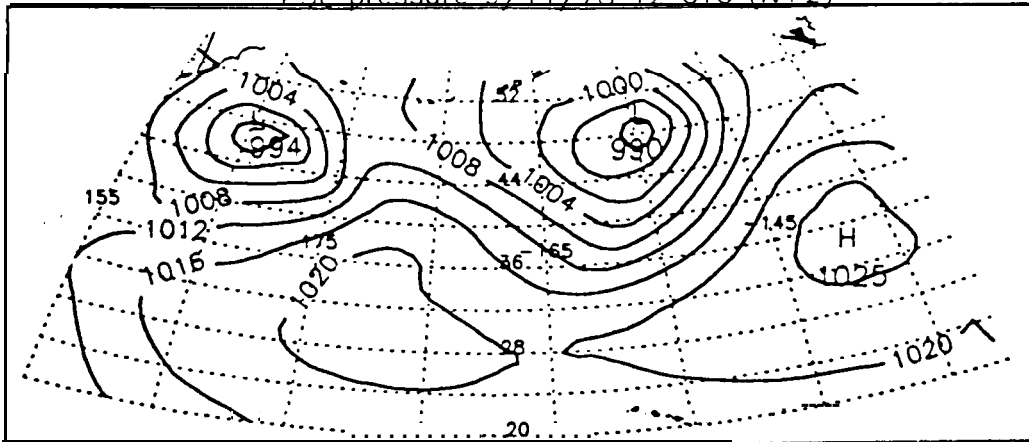


18Z14 SEPT 1978

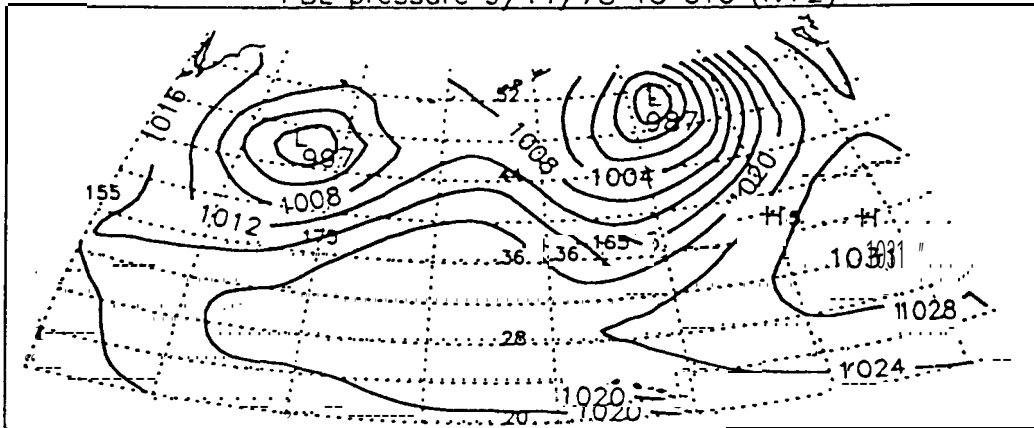
REV 1140



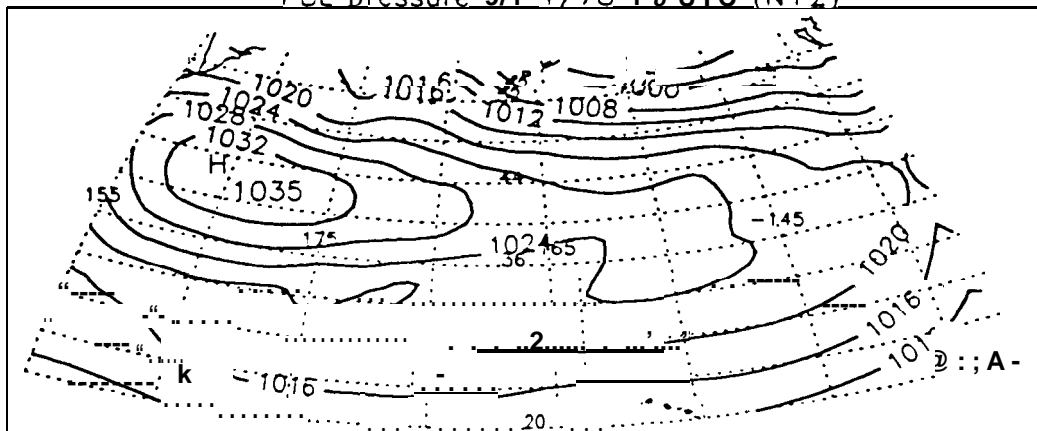
PBL pressure 9/11/78 12 UTC (N+2)

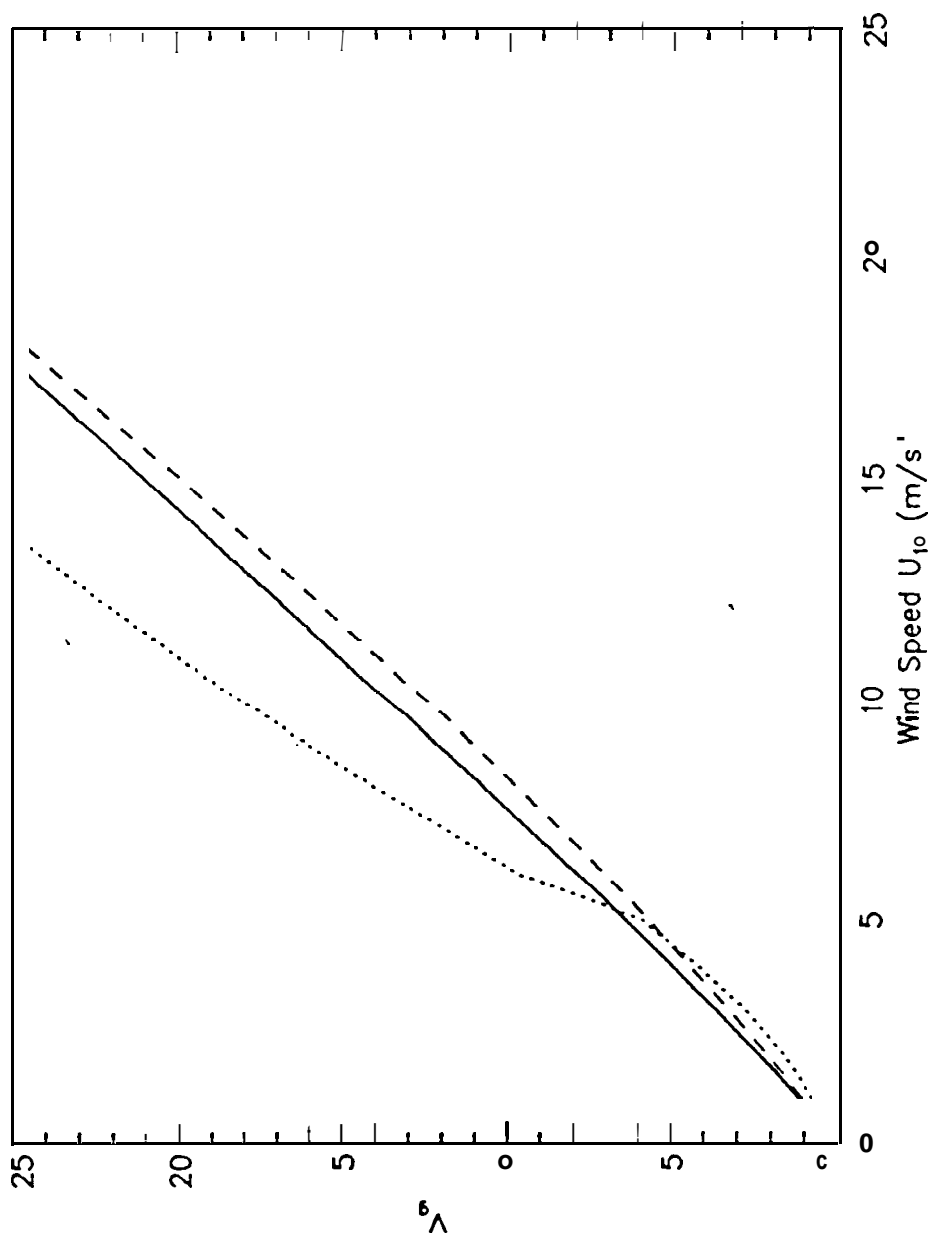


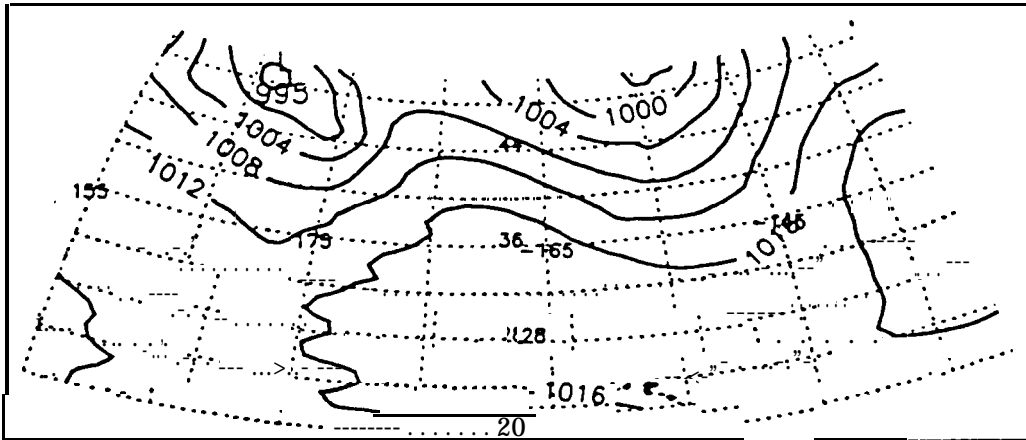
PBL pressure 9/11/78 18 UTC (N+2)



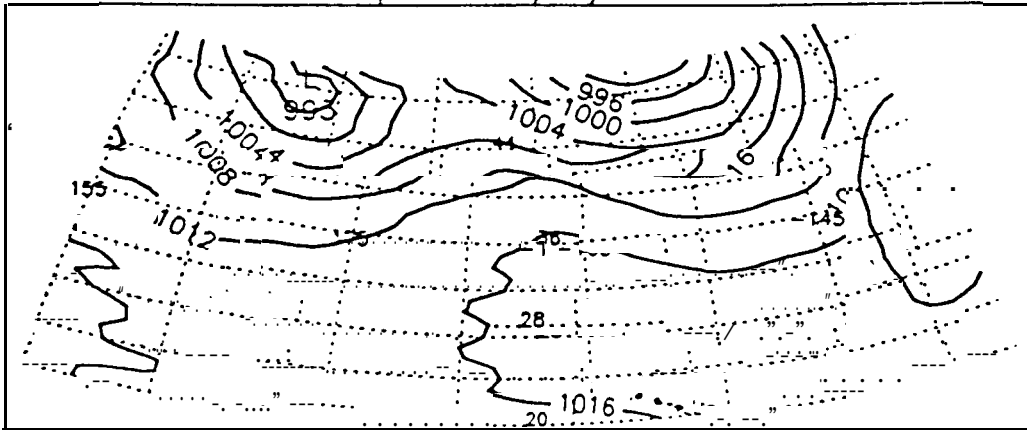
PBL pressure 9/14/78 18 UTC (N+2)



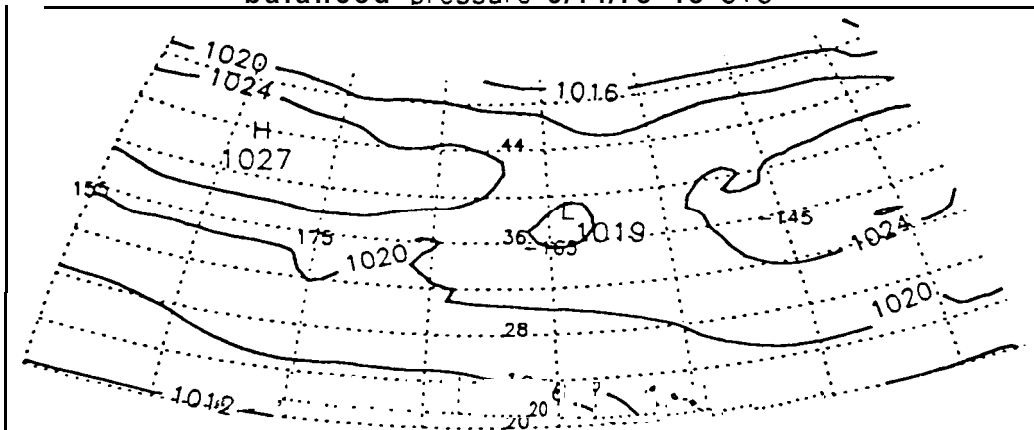




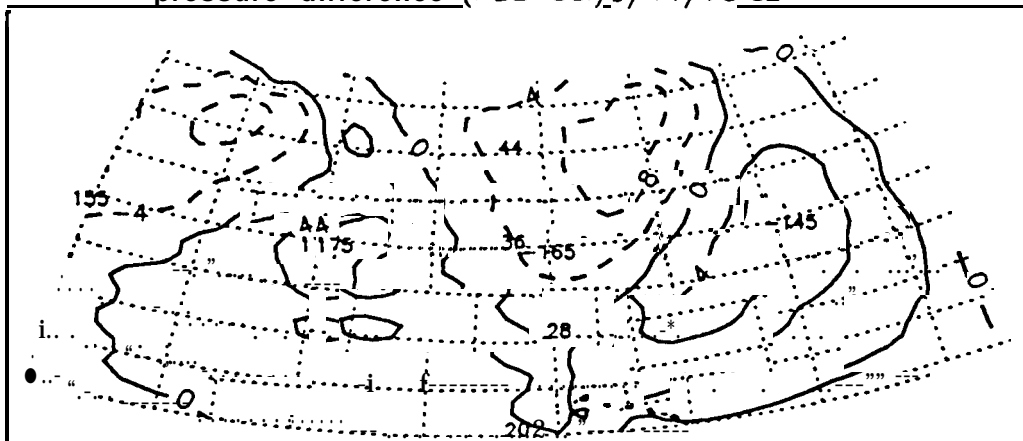
balanced pressure 9/11/78 18 UTC



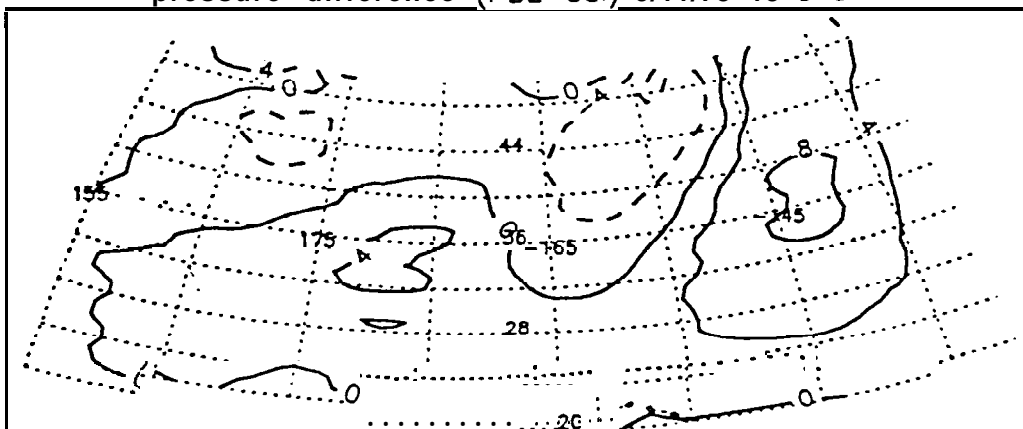
balanced pressure 9/14/78 18 UTC



pressure difference (PBL-bal) 9/11/78 12 UTC



pressure difference (PBL-bal) 9/11/78 18 UTC



pressure difference (PBL-bal) 9/14/78 18 UTC

